Chem. Res. Chinese Universities, 2019, 35(3), 485—489 doi: 10.1007/s40242-019-8332-1

Decomposition Mechanism of 5,5′-Bis(tetrazole)-1,1′-diolate(TKX-50) Anion Initiated by Intramolecular Oxygen Transfer

ZHAO Shengxiang[1], ZHAO Ying[2], XING Xiaoling[1] and JU Xuehai[2*]

1. Xi'an Modern Chemistry Research Institute, Xi'an 710065, P. R. China;

2. School of Chemical Engineering, Nanjing University of Science and Technology, Nanjing 210094, P. R. China

Abstract Density functional theory calculations at the B3LYP/6-31+G** and B3LYP/6-311++G** levels were performed on thermal decomposition of 5,5′-bis(tetrazole)-1,1′-diolate(TKX-50) anion with an intramolecular oxygen transfer being an initial step. The results show that the intramolecular oxygen transfers are the rate-limiting steps for the decomposition of title anion with activation energies being in the range of 287—328 kJ/mol. Judged by the nucleus-independent chemical shift values, the formation of antiaromatic ring in transition state or the decrease of aromaticity of the tetrazole ring of the reactant makes somewhat contribution to the high potential energies of the rate-limiting transition states. However, the activation energies of the following N_2 elimination through various pathways are in a low range of 136—166 kJ/mol. The tetrazole ring acts as an electron donor or acceptor in different pathways to assist the bond rupture or group elimination. The rate constants in a temperature range of 500—2000 K for all the intramolecular oxygen transferring reactions were obtained. The corresponding linear relationships between ln$k$ and 1/T were established.

Keywords Thermal decomposition; 5,5′-Bis(tetrazole)-1,1′-diolate(TKX-50) anion; Activation energy barrier; Density functional theory

1 Introduction

Energetic salts with high nitrogen contents have drawn much attention in recent years because their overall-properties could be improved by the chemical modification of both ions[1—3]. The Coulomb interaction between anions and cations endows the energetic salts with high density and stability in comparison with their atomically similar nonionic analogues. Fischer *et al*.[4,5] synthesized an energetic salt of dihydroxylammonium 5,5′-bistetrazole-1,1′-diolate(also named TKX-50) that has higher detonation velocity but lower sensitivity than commonly used high energy explosives, such as cyclotetramethylenetetranitramine(HMX), indicating that TKX-50 is a promising insensitive high energetic material. To probe insight into the microscopic mechanism of its thermal decomposition, some investigations have been conducted to characterize the behaviors at high temperatures with both theoretical and experimental methods.

Lu *et al*.[6] examined the protonation of the hydroxylammonium cation of TKX-50 by density functional theory method and found that a bimolecular reaction between two same sign charged ions under heating served as a dominant initial step in the thermal decay. An *et al*.[7] studied the atomistic reaction mechanisms for the initial decompositions of this system at high temperatures by the quantum mechanics. They found that continuous heating of the periodic system led eventually to the dissociation of the protonated or deprotonated bistetrazole to release N_2 and N_2O. These previous investigations showed that both the cation and anion could decompose independently or cooperatively. The anion of TKX-50 has high symmetry as well as strong conjugation of π electrons. The high symmetry is easy to eliminate in the process of thermal decomposition at high temperatures. One way of the symmetry losing is by the intramolecular oxygen transfer from one ring to another or within the same ring, in which the conjugation of the anion keeps. Although there is no evidence of such intramolecular oxygen transfers in TKX-50 yet, the experimentalists have found these phenomena in other molecules. Nakamura *et al*.[8] found that the intramolecular oxygen transfer from a carbonyl oxide moiety to a methoxyvinyl group was a highly efficient process and the demonstrated carbonyl oxides were not poor reagents for the epoxidation of electron-rich olefins. Lohrey *et al*.[9] found that oxygen atom transfer could lead to the formation of a phosphine-supported Re(III) BDI[N,N′-bis(2,6-diisopropylphenyl)-β-diketiminate] complex. Guo *et al*.[10] studied an intramolecular oxygen transfer reaction in the gas-phase dissociation of protonated sulfonamides and proposed a mechanism involving a three-membered ring transition state for the generation of the fragment ion $RC_6H_4O^+$. As can be seen in these systems, the intramolecular oxygen transfer played an

*Corresponding author. Email: xhju@njust.edu.cn

Received October 15, 2018; accepted January 22, 2019.

Supported by the Postgraduate Innovation Project of Jiangsu Province, China.

important role in the property and reactivity. In this paper, the thermal decomposition of TKX-50 anion initiated by an oxygen transfer was investigated by the density functional theory method. The optimized structures of all stationary states and energies along reaction pathways were analyzed. The changes of aromaticity for the initial key steps were analyzed. Rate constants for rate-limiting steps were predicted.

2 Computational Details

The initial molecular structures were constructed by Chem3D software. The molecular structures were optimized and the energies of the reaction stationary points were determined by the efficient density functional theory(DFT) method[11,12]. The density functional theory methods that not only produce reliable geometries and energies but also require less time and computer resources, have been widely employed and have become an important and economical tool to deal with complex electron correlation-problems of molecules and reactions[13—17]. The geometries of all the species(reactants, intermediates, transition states and products) were optimized at the B3LYP/6-31+G** and B3LYP/6-311++G** levels. Single point calculations at the MP2/6-311++G** level were performed to confirm the validation of DFT results. The vibrational frequencies were calculated at the same level. There was only one imaginary frequency for each transition states that was further verified to connect the designated reactants with products by performing an intrinsic reaction coordinate(IRC) analysis. All the calculations were performed with Gaussian 09 package of programs[18].

3 Results and Discussion

3.1 Optimized Structures and Energies Along Reaction Pathways

Fig.1 shows the structures from reactant to products by three routes. The relative energies for all species along the reaction pathways are displayed in Fig.2. As seen from Fig.2, the energy barriers of the transition states at the B3LYP/6-31+G** and B3LYP/6-311++G** levels are consistent with each other as a whole, indicating the basis sets used approach to the limit.

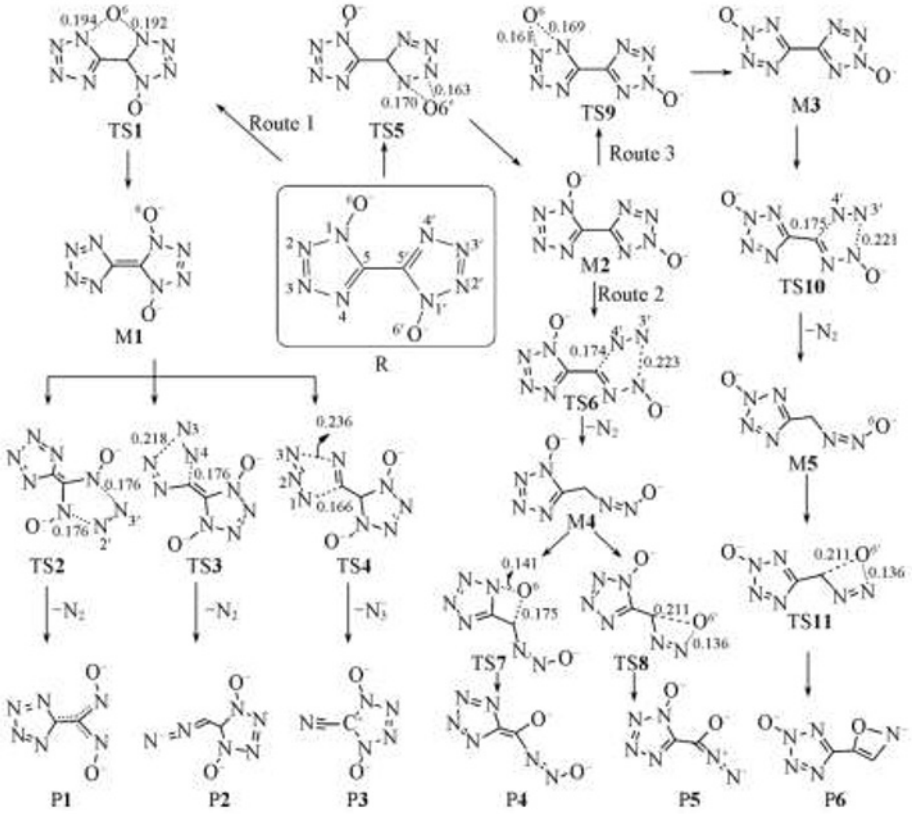

Fig.1 Atomic numbering of reactant(R) and structural changes along reaction pathways

Route 1 generates isomer M**1** from R that decomposes into products P**1**, P**2** and P**3**; route 2 generates isomer M**2** that decomposes to P**4** and P**5**; route 3 generates isomer M**3** that produces P**6**. Data in nm on the bonds of transition states were from B3LYP/6-311+G** level.

The geometrical structures and energies hereafter refer to the results at the B3LYP/6-311++G** level unless otherwise stated. The decomposition of the 5,5′-bis(tetrazole)-1,1′-diolated anion was initiated by three routes of intramolecular oxygen transferring: an oxygen atom of one tetrazole ring transferring to another ring, an oxygen atom transferring within the ring to its neighbor nitrogen and one more oxygen atom transferring within the ring, followed by the decomposition of intermediates(M**1**, M**2** and M**3** as shown in Fig.1). In Route 1, one oxygen in one tetrazole ring transfers to another tetrazole ring through TS**1**, which leads to the formation of M**1**. TS**1** has a five-number ring with considerable energy barrier of 369.35 kJ/mol at the B3LYP/6-311++G** level(Fig.2). The transferring oxygen atom in TS**1** connects to two nitrogen atoms of the

respective tetrazoles with almost identical bond lengths of 0.19 nm. M**1** decomposes by three pathways through TS**2**, TS**3** and TS**4**, releasing nitrogen gas or azide anion. Although both TS**2** and TS**3** release N_2, the energy barrier of TS**2**(136.31 kJ/mol) is less than that of TS**3**(166.61 kJ/mol) by 30 kJ/mol since the ruptures of both N—N bonds with identical length of 0.176 nm in TS**2** are concerted. The N_3^- elimination of M**1** *via* 5-centered TS**4** has a larger barrier of 185.20 kJ/mol than that of N_2 elimination.

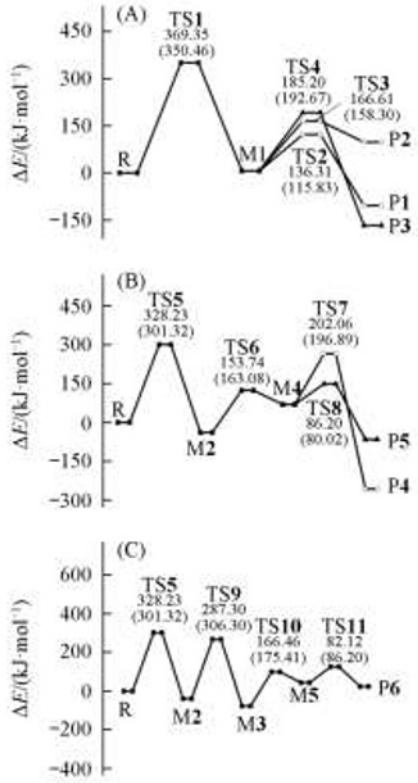

Fig.2 Energy changes along the reaction pathways of Route 1(A), Route 2(B) and Route 3(C) at B3LYP level with basis sets of 6-31+G(in parentheses) and 6-311++G****

The oxygen transfer to an *ortho*-position within one tetrazole ring leads to the formation of M**2** *via* TS**5**(328.23 kJ/mol). M**2** decomposes either *via* TS**6**(153.74 kJ/mol), or *via* another step of *ortho*-position oxygen transfer within the other tetrazole ring(TS**9**, 287.30 kJ/mol). The former denotes as Route 2 and the latter Route 3. In Route 2, one of the tetrazole rings opens to release N_2 *via* TS**6**(153.74 kJ/mol). The intermediate undergoes an oxygen transferring from N-position to C-position by the four-center transition states of TS**7** and TS**8**, with reaction barriers of 202.06 and 86.20 kJ/mol, respectively. The ring open product with oxygen attached to carbon is expected to release CO, N_2O and NO through further decomposition, judged by their molecular structures of P**4** and P**5**.

In Route 3, another oxygen transfers to its *ortho*-position *via* TS**9**(287.30 kJ/mol), leading to the formation of M**3**. M**3** releases N_2 *via* TS**10**(166.46 kJ/mol) and forms a ring open product, in which the oxygen transfers from N-position to C-position readily by a four-center transition state of TS**11**(82.12 kJ/mol) and generates a ring close product P**6**. To verify the reliability of the DFT results, single-point calculations at MP2/6-311++G** level were performed on the basis of the optimized geometries at the B3LYP/6-311++G** level. Most of the discrepancies for the activation energies between the MP2 and B3LYP levels are within 10 kJ/mol, with the largest one of 18.5 kJ/mol(Table S1, see the Electronic Supplementary Material of this paper). Thus, the results from the two levels are in good agreement with each other.

It is well known that benzene is stabilized by its aromaticity. In order to elucidate the original of the variation of reaction energies, we also investigated the aromaticity of the reactant and the transition states for the rate-limiting steps. Based on the nucleus-independent chemical shift(NICS) theory[19,20], the $NICS(0)_{zz}$ was calculated at the B3LYP/6-311++G** level for R, TS**1** and TS**5**. As seen in Fig.3, the $NICS(0)_{zz}$ in both rings of R is δ –10.4, which is close to that of benzene[19], indicating that these rings are strongly aromatic. The $NICS(0)_{zz}$ values of both tetrazole rings in TS**1** decrease compared to that of R, but its five-center ring of transition state has a positive $NICS(0)_{zz}$ value. The antiaromaticity of the latter moiety leads to the large activation energy of TS**1**. The $NICS(0)_{zz}$ values of one tetrazole ring in TS**5** becomes δ –4.5, which decreases the stability of TS**5**.

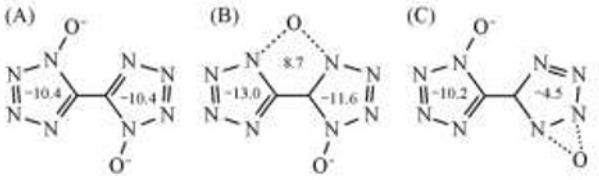

Fig.3 $NICS(0)_{zz}$ values at ring critical points of reactant(A) and transition states TS1(B) and TS5(C)

The intramolecular oxygen transfers are the rate-limiting steps for the decomposition of title anion with reaction activation energies being in a range of 287—328 kJ/mol. The formation of antiaromatic ring in transition state or the decrease of the original aromaticity of reactant makes somewhat contribution to the high potential energies of the rate-limiting transition states. However, the activation energies of thereafter N_2 elimination through various pathways(by TS**2**, TS**3**, TS**6** and TS**10**) are in a low range of 136—166 kJ/mol, which are less or much less than 189 kJ/mol at the same computational level for the direct N_2 elimination of the anion[7].

3.2 Charge Transfer

Table 1 lists the atomic Mülliken charges of all the stationary points along the reaction pathways at the B3LYP/6-311++G** level. The negative charges of 5,5′-bis(tetrazole)-1,1′-diolated anion(R in Fig.1) are mainly distributed on the oxygen atoms, with the second largest negative charge on N4—C5(N4′—C5′). In TS**1** of Route 1, the negative charges centralize on nitrogen atoms that connect to oxygen atom with almost identical distance of 0.19 nm(Fig.1) when the oxygen transfers from N1 to N4′. For M**1**, the negative charges distribute mainly on two oxygen atoms and N1—C5—N4. The total charges of non-oxygen tetrazole ring

are 0.82 e, indicating the oxygen remains most of its negative charges on the original tetrazole that releases nitrogen gas *via* TS**2** and gives rise to P**1**. The total charges on the tetrazole ring of P**1** are −1.37 e, since the conjugation effect of tetrazole ring is favorable to accept electron and lowers the electron energy. When M**1** releases nitrogen gas *via* TS**3** and gives rise to P**2**, the positively charged nitrogen atom in the ruptured ring withdraws electrons from the diolated ring. As a result, the total charges on the diolated ring are only –0.95 e although the ring has two oxygen atoms. The elimination of azide anion from M**1** *via* TS**4** is accompanied by the electron transfer from diolated ring to the leaving group of azide anion, resulting in the total charges on the diolated ring of P**3** being as small as −0.25 e and total charges on the five-center tetrazole ring being 0.11 e. Compared with M**1**, the tetrazole ring of P**3** acts as an electron donor.

Table 1 Atomic Mülliken charges along reaction pathways at B3LYP/6-311++G level**

Species	Q_{N1}/e	$Q_{N1'}$/e	Q_{N2}/e	$Q_{N2'}$/e	Q_{N3}/e	$Q_{N3'}$/e	Q_{N4}/e	$Q_{N4'}$/e	Q_{C5}/e	$Q_{C5'}$/e	Q_{O6}/e	$Q_{O6'}$/e
R	–0.06	–0.06	–0.06	–0.06	–0.10	–0.10	–0.22	–0.22	–0.23	–0.23	–0.33	–0.33
TS**1**	–0.44	–0.28	0.05	–0.09	–0.07	–0.03	–0.26	–0.40	–0.16	–0.01	–0.06	–0.26
TS**2**	–0.23	–0.05	–0.06	–0.14	–0.06	–0.14	–0.23	–0.05	–0.29	–0.22	–0.28	–0.28
TS**3**	0.13	–0.15	–0.29	–0.12	–0.14	–0.10	–0.14	–0.19	–0.52	0.02	–0.26	–0.25
TS**4**	–0.13	–0.14	0.05	–0.11	–0.22	–0.11	–0.28	–0.14	–0.59	0.21	–0.26	–0.26
TS**5**	–0.17	–0.20	–0.01	0.17	–0.06	–0.17	–0.30	–0.07	–0.14	–0.40	–0.33	–0.31
TS**6**	–0.04	0.22	–0.06	–0.20	–0.07	–0.08	–0.30	–0.12	–0.02	–0.66	–0.33	–0.35
TS**7**	–0.22	0.18	0.04	–0.37	–0.19	0	–0.17	0	–0.33	–0.44	–0.09	–0.41
TS**8**	0.02	0.09	–0.16	0.24	–0.12	0	–0.23	0	–0.18	–0.47	–0.29	–0.41
TS**9**	–0.24	–0.15	0.20	–0.18	–0.03	0.15	–0.22	–0.37	–0.01	–0.50	–0.32	–0.33
TS**10**	–0.06	0.23	–0.21	–0.20	0.13	–0.14	–0.34	–0.17	–0.30	–0.39	–0.31	–0.35
TS**11**	–0.04	0.10	–0.19	–0.25	0.09	0	–0.31	0	–0.28	–0.41	–0.32	–0.40
M**1**	–0.22	–0.15	–0.06	–0.10	–0.06	–0.10	–0.22	–0.15	–0.26	–0.15	–0.26	–0.26
M**2**	–0.32	–0.16	0.07	–0.21	–0.02	0.20	–0.35	–0.35	0.31	–0.56	–0.30	–0.31
M**3**	0.09	–0.09	–0.20	–0.20	0.12	0.12	–0.32	–0.32	–0.18	–0.18	–0.33	–0.33
M**4**	0	0.61	–0.16	–0.50	–0.03	0	–0.39	0	–0.03	–0.73	–0.32	–0.45
M**5**	–0.07	0.60	–0.20	–0.47	0.15	0	–0.40	0	–0.23	–0.59	–0.33	–0.45
P**1**	–0.17	–0.19	–0.09	0	–0.09	0	–0.17	–0.19	–0.85	0.16	–0.21	–0.21
P**2**	0.50	–0.08	–0.61	–0.22	0	–0.06	0	–0.40	–0.94	0.41	–0.28	–0.31
P**3**	–0.69	–0.25	0.39	–0.06	–0.69	–0.06	–0.33	–0.25	–0.41	0.73	–0.18	–0.18
P**4**	–0.22	0.14	–0.09	–0.38	–0.03	0	–0.33	0	–0.01	–0.39	–0.36	–0.34
P**5**	–0.05	0.37	–0.14	–0.61	–0.11	0	–0.25	0	–0.16	–0.16	–0.34	–0.58
P**6**	–0.12	–0.28	–0.24	–0.25	0.09	0	–0.37	0	–0.43	0.16	–0.35	–0.21

During the oxygen transfer to its *ortho*-position in the process of R isomerizing to M**2** *via* TS**5**, the main electron transferring is from C5 to C5′. The charges on C5 change from –0.23 e to 0.31 e and the total charges on this ring are –0.61 e, while those on C5′ are from –0.23 e to –0.56 e. After the elimination of N_2 from M**2** *via* TS**6**, the total charges of the oxidized tetrazole ring become –0.93 e, indicating the electron withdraws to the sole conjugated ring. There are two paths for oxygen transfer from nitrogen to carbon *via* TS**7** and TS**8**, with the formation of C—O bond. The total charges on the tetrazole ring of P**4** are –0.68 e. Although there is no oxygen atom in the ring of P**4**, its conjugation effect enables it to accept electron favorably. The total charges on the oxidized tetrazole ring of P**5** are –1.05 e.

In Route 3, the electron on C5′ transfers back to C5 when M**2** isomerizes to M**3** *via* TS**9**. The elimination of N_2 from M**3** *via* TS**10** hardly affects the total charges on the oxidized tetrazole ring. A ring close reaction of M**5** takes place *via* TS**11**, resulting in a more even charge distribution in P**6**.

3.3 Rate Constants

In order to obtain the rate constants for the rate-limiting steps, *i.e.*, the intramolecular oxygen transfers *via* TS**1**, TS**5** and TS**9**, the transition state theory of Eyring was used to calculate the rate constant by the following equation:

$$k = \frac{k_B T}{\hbar}\left(\frac{p^\theta}{RT}\right)^{1-n}\exp\left(\frac{\Delta^{\neq}S^\theta}{R}\right)\exp\left(\frac{-\Delta^{\neq}S^\theta}{RT}\right)$$

where the k_B and $\hbar$ are the Boltzmanm and Plank constants, $\Delta^{\neq}S^{-\theta}$ and $\Delta^{\neq}H^{-\theta}$ are the activation entropy and activation enthalpy of a reaction under the condition of $p^{-\theta}$=100 kPa, n is the sum of computation coefficients for all the reactants, and n=1 here for intramolecular oxygen transferring process.

Fig.4 shows the rate constants in a temperature range of 500—2000 K. There are linear relationships between ln$k$ and 1/T for all the intramolecular oxygen transferring reactions. Rate constants of the reaction with TS**1** increase more greatly than those of the other two. Under 1050 K, the rate constants of

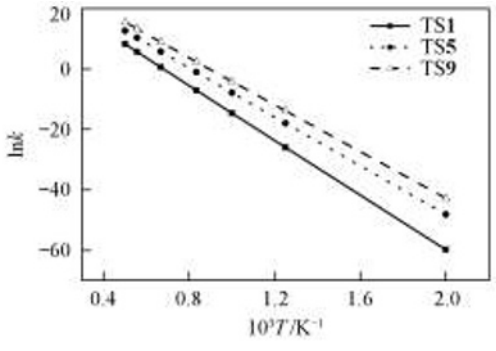

Fig.4 Relationship of ln$k$ and 1/T in oxygen transfer reaction at B3LYP/6-311++G level**

all the intramolecular oxygen transferring are less 0.1 s^{-1}, indicating that these reactions take place by low rates. However, k_{TS1}=0.2 s^{-1} when the temperature is 1400 K, indicating that all the intramolecular oxygen transferring reactions occur at a considerable rate over 1400 K. Since such high temperatures prevail at the later stage of combustion or detonation[21], the decomposition initiated by the intramolecular oxygen transfer will be triggered consequently.

4 Conclusions

From the density functional theory calculations on the thermal decomposition of 5,5′-bis(tetrazole)-1,1′-diolate(TKX-50) anion, we concluded that there are three main routes for the decomposition of the anion with an intramolecular oxygen transfer being an initial step. The rate-limiting steps are the intramolecular oxygen transfers with activation energies in the range of 287—328 kJ/mol. On the contrary, the activation energies of N_2 elimination thereafter through various pathways are in a low range of 136—166 kJ/mol. All the intramolecular oxygen transferring reactions occur at a considerable rate over 1400 K. The decomposition initiated by the intramolecular oxygen transfer will be triggered at the later stage of combustion or detonation when high temperature prevails.

Electronic Supplementary Material

Supplementary material is available in the online version of this article at http://dx.doi.org/10.1007/s40242-019-8332-1.

References

[1] Klapötke T. M., Witkowski T. G., *Propel. Explos. Pyrotech*., **2016**, *41*(3), 470

[2] Meng Z. Y., Zhao F. Q., Xu S. Y., Ju X. H., *Can. J. Chem.*, **2017**, *95*, 691

[3] Xu Z., Cheng G. B., Yang H. W., Ju X. H., Yin P., Zhang J. H., Shreeve J. M., *Angrew. Chem. Int. Ed*., **2017**, *56*(21), 5877

[4] Fischer N., Fischer D., Klapötke T. M., Piercey D. G., Stierstorfer J., *J. Mater. Chem*., **2012**, *22*, 20418

[5] Fischer N., Klapötke T. M., Reymann M., Stierstorfer J., *Eur. J. Inorg. Chem*., **2013**, *2013*(12), 2167

[6] Lu Z. P., Xiong Y., Xue X. G., Zhang C. Y., *J. Phys. Chem. C*, **201**7, *121*(50), 27874

[7] An Q., Liu W., William A. G., Cheng T., Zybin S. V., Xiao H., *J. Phys. Chem. C*, **2014**, *118*, 27175

[8] Nakamura N., Nojima M., Kusabayashi S., *J. Am. Chem. Soc*., **1986**, *17*(48), 4969

[9] Lohrey T. D., Bergman R. G., Arnold J., *Inorg. Chem.*, **2016**, *55*(22), 11993

[10] Guo N., Shen S. S., Song W. W., *Int. J. Mass Spectrometry*, **2019**, *435*, 124

[11] Seminario J. M., Politzer P., *Modern Density Functional Theory: a Tool for Chemistry*, Elsevier, Amsterdam, **1995**

[12] Lee C., Yang W., Parr R. G., *Phys. Rev. B*, **1988**, *37*(2), 785

[13] Huang S. Q., Zeng X. L., Xu S.Y., Ju X. H., *Comput. Theor. Chem.*, **2016**, *1093*, 91

[14] Fariba M., Mahshid H., *Struct. Chem*., **2018**, *29*(1), 9

[15] Zhao K., Yu X., Chen L., Hou H., Jiang Y., Zhang C., Wang B., *Comput. Theor. Chem.*, **2016**, *1096*, 80

[16] Monia C., Hammouda C., Hedi M., Youssef A., *Chem. Res. Chinese Universities*, **2017**, *33*(5), 765

[17] Zhang H. M., Liu Y., Ma F. P., Qiu W., Lei B., Shen J. Y., Sun X.Y., Han W. Q., Li J. S., Wang L. J., *Chem. Res. Chinese Universities*, **2017**, *33*(5), 785

[18] Frisch M. J., Trucks G. W., Schlegel H. B., Scuseria G. E., Robb M. A., Cheeseman J. R., Scalmani G., Barone V., Mennucci B., Petersson G. A., Nakatsuji H., Caricato M., Li X., Hratchian H. P., Izmaylov A. F., Bloino J., Zheng G., Sonnenberg J. L., Hada M., Ehara M., Toyota K., Fukuda R., Hasegawa J., Ishida M., Nakajima T., Honda Y., Kitao O., Nakai H., Vreven T., Montgomery J. A. Jr., Peralta J. E., Ogliaro F., Bearpark M., Heyd J. J., Brothers E., Kudin K. N., Staroverov V. N., Kobayashi R., Normand J., Raghavachari K., Rendell A., Burant J. C., Iyengar S. S., Tomasi J., Cossi M., Rega N., Millam J. M., Klene M., Knox J. E., Cross J. B., Bakken V., Adamo C., Jaramillo J., Gomperts R., Stratmann R. E., Yazyev O., Austin A. J., Cammi R., Pomelli C., Ochterski J. W., Martin R. L., Morokuma K., Zakrzewski V. G., Voth G. A., Salvador P., Dannenberg J. J., Dapprichm S., Daniels A. D., Farkas O., Foresman J. B., Ortiz J. V., Cioslowski J., Fox D. J., *Gaussian* 09, Gaussian Inc., Wallingford, **2009**

[19] Schleyer P. V. R., Maerker C., Dransfeld A., Jiao H., *J. Am. Chem. Soc*., **1996**, *118*(26), 6317

[20] Báezgrez R., Ruiz L., Pinorios R., Tiznado W., *RSC Adv.*, **2018**, *8*(24), 13446

[21] Grys S., Trzciński W. A., *Cent. Eur. J. Energ. Mater.*, **2010**, *7*(2), 97